Theoretical Study in the Realization of Real-Time Parallel Optical Logic Operations Using Two-Wave Mixing in Photorefractive Materials

R.S. Fyath[*], *J.M. Abdul-Jabbar*[**] *and S.M. Ameen*[***]

[*]*Department of Electrical Engineering, College of Engineering,*
[**]*Department of Computer Engineering, College of Engineering,*
[***]*Department of Physics, College of Science, University of Basrah, Basrah, Iraq.*

ABSTRACT

A theoretical analysis is presented to calculate the signal phase shift and the gain coefficient associated with two-wave mixing in photoreftactive crystals subjected to an external electric field. The relative position of the induced-refractive index grating with respect to the fringe pattern of the two input optical beams leads to coupling effect between the phase and intensity of these beams.

An optical logic operation system that is based on photorefractive two-wave mixing is introduced. This system uses the fringe-shifting techniques that are executed by a Mach-Zehnder interferometer. The proposed system configurations are capable of producing all the basic 16 two-operand Boolean functions simultaneously at different output planes.

دراسة نظرية في تصميم دوائر منطق ضوئية في الزمن الحقيقي باستخدام تقنية مزج الموجتين في المواد الحساسة للضوء

يقدم البحث دراسة نظرية لحساب فرق الطور وعامل التضخيم المصاحب لعمليـة مـزج موجتين ضوئيتين في المواد الحساسة للضوء عند تعرضها لمجال كهربائي خارجي. تسم استخدام النتائج في تصميم نظام له القابلية على توليد الست عشر دائرة منطقية الخاصـة بادخالين في الزمن الحقيقي باستخدام مستويي اخراج.

1. INTRODUCTION

Parallel optical logic gates are fundamental for optical computing. Recently, various devices that are based on different spatial light modulators (SLMs) have been implemented[1-3]. Among these SLMs, the photorefractive crystals attract increasing interest for optical data processing and computing due to their real time capabilities and parallelism [4,5].

Photorefractive effect means the purely refractive-index modulation produced by using the linear electro-optic effect arising from a photoinduced space-charge electric field distribution. Charge carriers are generated by photon absorption in the illuminated regions of the crystal. The electrons are free to migrate through the crystal until they are retrapped in the dark regions. The periodic distribution of the retrapped electrons generates periodic space-charge field which modulates the refractive index, via the electro-optic effect, forming a phase grating which

corresponds to the original light intensity distribution. When the crystal is illuminated by two optical beams, the phase grating may be shifted with respect to the interference pattern due to different mechanics of carrier transportation. This phase shift is the source of an energy redistribution between the two beams.

For materials with large electro-optic coefficients (r_{eff}), such as $BaTiO_3$ (BTO) and $KNbO_3$, the predicted gain coefficient is ~ 5 cm^{-1} which exceeds the typical attenuation coefficient. Thus these materials can be used as optical amplifiers [6] and in real-time optical image-processing devices that require gain[7,8]. On the other hand, materials with relatively small electro-optic coefficients, such as $Bi_{12}SiO_{20}$ (BSO), $Bi_{12}GeO_{20}$ (BGO) and GaAs have many advantages for real-time optical data processing [9] and holographic storage [10], such as fast response, large photorefractive sensitivity, and are readily available in large crystals[10]. The small electro-optic coefficient in these materials can be compensated for by applying uniform electric field (of the order of 2-20 kV/cm)[11].

In this paper, a theoretical analysis based on the charge-transport model is presented to assess the gain coefficient and phase shift associated with photorefractive two-wave mixing. The simulation results obtained for BSO crystal is used as a guideline to design a real-time optical parallel logic operation system capable of producing the sixteen basic two-operand logic functions simultaneously.

2. PHOTOREFRACTIVE TWO-WAVE MIXING

2-1. Theory

The sillenite BSO crystal is a paraelectric electro-optic and photoconductive material. It has a cubic point group symmetry and therefore it is optically isotropic if no electric field is applied. With the application of an electric field, BSO crystal becomes birefringent due to nonvanishing Pockel's coefficient $r_{eff}=r_{41}=5$ pm/V. The geometry shown in Fig.1 gives better coupling between recording beams and it is used in light amplification or optical phase conjugation. The refractive index modulation in such geometry is given by

$$\Delta n = \frac{1}{2}\, r_{41}\, n_o^3\, E \qquad (1)$$

where r_{41} is the electro-optic coefficient, E is the space-charge or any modulation field, n_o is the background refractive index of the crystal.

The factor δ, that expresses the electro-optic activity of the crystal, depends on the symmetry of the material. For the geometry given in Fig.1, δ is given by [11]

$$\delta = \frac{\pi\, n_o^3\, r_{41}}{\lambda_o \cos\theta} \qquad (2)$$

where λ_o is the wavelength of the input optical beams, and 2θ is the angle between the two beams.

Consider two monochromatic coherent light beams, the pump $\mathbf{P}\, e^{-i\omega t}$ and signal $\mathbf{S}\, e^{-i\omega t}$, with wave vectors $\mathbf{k_p}$ and $\mathbf{k_s}$ incident symmetrically on a slab of non-absorbing photorefractive material with the configuration shown in Fig.1. For simplicity, $\mathbf{P}$ and $\mathbf{S}$ are assumed to be polarized normal to the plane of incidence with

$$\mathbf{P} = \hat{e}_x\, P(z,t)\, e^{-i\,\mathbf{k_p}\cdot\mathbf{r}} \qquad (3)$$

$$\mathbf{S} = \hat{e}_x\, S(z,t)\, e^{-i\,\mathbf{k_s}\cdot\mathbf{r}} \qquad (4)$$

where P(z,t) and S(z,t) are complex amplitudes of the pump and signal waves, respectively, which vary along the z direction and have time dependency because of the energy coupling effects as a result of the interaction with the grating. It is convenient to write

$$P(z,t) = \sqrt{I_p(z,t)}\, e^{i\varphi_p(z,t)} \qquad (5)$$

$$S(z,t) = \sqrt{I_s(z,t)}\, e^{i\varphi_s(z,t)} \qquad (6)$$

where I_S, I_P, φ_p and φ_s are real values.

The intensity distribution in the fringe pattern within the crystal is then described by the expression,

$$I_{int}(x,y,z,t) = (E_{opt} \cdot E^{*}_{opt}) = |P+S|^2 \qquad (7)$$

where $\langle\ \rangle$ denotes the average and E_{opt} is the total optical electric field in the medium which is given as,

$$E_{opt}(x,y,z,t) = \hat{e}_x \left[P(z,t)\, e^{-i k_o y} + S(z,t)\, e^{+i k_o y}\right] \qquad (8)$$

Therefore, the total optical irradiance in the crystal is given by,

$$I_{tot}(y,z,t) = I_o \left(1 + 2\frac{\sqrt{(I_p I_s)}}{I_o} \cos(2k_o y \sin\theta + \Delta\varphi)\right) \qquad (9)$$

where $I_o = I_P + I_S$ is the total intensity of the incident beams and $\Delta\varphi = \varphi_p - \varphi_s$

Consequently, space-charge fields are generated which induce a periodic refractive index change, via the electro-optic effect. The periodic index change gives the crystal its diffraction properties (see the Appendix for details). The fringe spacing (refractive-index grating period) is given by

$$\Lambda = \frac{\lambda_o}{2 n_o \sin\theta} \qquad (10)$$

The phase shift introduced to the signal optical field, after passing a crystal of thickness z=d, is given by

$$\Delta\varphi_s = \varphi_s(d) - \varphi_s(0)$$

$$\Delta\varphi_s = \delta E_q\, d + \frac{\cot\varphi_g}{2} \ln\left[\frac{(\beta_o + 1)\, e^{\Gamma d}}{\beta_o + e^{\Gamma d}}\right] \qquad (11)$$

Where

$$\beta_o = \left.\frac{I_p}{I_s}\right|_{z=0} \qquad (12)$$

$$\Gamma = 2\delta E_q \frac{1 + E_d/E_q + E_o^2/E_d E_q}{(1 + E_d/E_q)^2 + (E_o/E_q)^2} \qquad (13)$$

$$\phi_g = \tan^{-1}\left[\frac{E_d(1 + E_d/E_q + E_o^2/E_d E_q)}{E_o}\right] \qquad (14)$$

$$E_d = \frac{2\pi k_B T}{\Lambda e} \qquad (15)$$

$$E_q = \frac{e \Lambda N_A}{2\pi \varepsilon_o \varepsilon} \qquad (16)$$

In eqs.(11)-(16),

- Γ ≡ Intensity gain coefficient.
- β_o ≡ Initial intensity ratio (Beam intensity ratio at z=0).
- E_o ≡ Applied electrical field.
- E_q ≡ Peak amplitude of the space-charge field.
- E_d ≡ Diffusion field.
- ϕ_g ≡ Phase shift of the space-charge field (Phase mismatch between space-charge field and fringe pattern).
- N_A ≡ Trap density.
- K_B ≡ Boltzman constant.
- ε ≡ Dielectric constant.
- Λ ≡ Fringe-spacing.
- e ≡ Electron charge.
- T ≡ Absolute temperature.

The amplitude of the index change follows the local visibility of the writing interference pattern, but that index maxima and intensity maxima are shifted in phase by an amount ϕ_g. Therefore, a precise knowledge of the phase shift ϕ_g, which can be measured as described in Ref.[12], is of fundamental significance for understanding the mechanism of the photorefractive effect.

2-2. Illustrative Results

Figures 2-7 show simulation results characterizing the two-wave mixing in BSO crystal. Unless otherwise stated, the parameter values used in the simulation are r_{41}=5 pm/V, n_o=2.54, N_A=9x10^{19} cm^{-3}, d=1.5 cm, θ=5°, λ_o=488 nm, and ε=56.

Figure 2 shows the gain (amplification) and the attenuation (depletion) seen by the signal and pump waves, respectively, as they passes through the crystal. The intensity of the signal beam grows with distance z as $I_s = I_o e^{\Gamma z}/(\beta_o + e^{\Gamma z})$ where I_o is

the total intensity of the incident beams. The pump is depleted according to $\beta_o I_o/(\beta_o + e^{\Gamma z})$. The two normalized intensity I_s/I_o and I_p/I_o are equal at a distance $z=(1/\Gamma)\ln\beta_o$. The gain coefficient Γ is estimated to be 1.5 cm^{-1} using the parameter values used in the simulation (E_o=10 kV/cm, $\theta=5°$, and $N_A=9\times10^{19}$ cm^{-3})

The dependence of the gain coefficient Γ on the angle θ is depicted in Fig.3. Note that Γ is an increasing function of θ. To get Γ =2.5 cm^{-1}, θ must be fixed at 8°. It is worth to mention here that Γ is almost independent of E_o when $N_A=9\times10^{19}$ cm^{-3} and Γ can be approximated by $2\delta E_d$ when $E_o<<E_q=5\times10^4$ kV/cm for $\theta=5°$.

The variation of the phase shift $\Delta\varphi_s$ with N_A, β_o, E_o and θ are depicted, respectively in Figs.4-7. Investigating these figures highlights the following findings.

(i) The phase shift is negligible when N_A is less than 10^{15} cm^{-3}.

(ii) The phase shift increases with increasing N_A till a saturation level is reached. To reach this level, high values of N_A is needed in the presence of high external field E_o.

(iii) $\Delta\varphi_s$ has a nonlinear dependence on β_o. For $\beta_o<2$, $\Delta\varphi_s$ varies almost linearly with β_o. However, it is worth to note that the nonlinear $\Delta\varphi_s$-β_o characteristics is useful to implement the optical logic operations.

(iv) $\Delta\varphi_s$ increases almost linearly with E_o and the proportionality constant is a decreasing function of θ. For example, when $\theta=5°$, $\Delta\varphi_s$= 2.3 π, and 4.61 π when E_o= 10, and 20 kV/cm, respectively. These results are to be compared with $\Delta\varphi_s$= 1.84 π and 3.68 π when E_o= 10 and 20 kV/cm, respectively, and assuming $\theta=10°$.

3. REALIZATION OF REAL-TIME OPTICAL LOGIC OPERATIONS

Table 1 lists the sixteen basic operations for two-operand Boolean algebra. These logic operations can be realized by using a photorefractive two-wave mixing system and fringe shifting technique. Several logic gates can be implemented simultaneously by using the system configuration proposed by Xu et al.[13] (see Fig.8a). Here, the two incident beams from the laser source interact at angle 2θ on BSO crystal. Two beam splitters (BS4 and BS5) and two mirrors (M5 and M6) constitute a Mach-Zehnder interferometer, which yields the initial phase variation $\phi_s(0)$ of the optical signal wave. The output signal intensity pattern at the output plane is described as

$$I_{out} = I_s + I_{so} + 2\sqrt{I_s I_{so}}\cos(\Delta\varphi_s) \qquad (16)$$

where $I_{so}=I_s(0)$, i.e., the intensity of the incident signal beam.

At the plane of the crystal, the pump beam intensity I_P is modulated by the sum of two binary input patterns A and B, which are combined by the beam splitter BS3. The interference fringes at the output plane are adjusted so that one period of the fringes corresponds to the width of an input pixel. The shift of the output fringe and the corresponding logic operation depend on the intensity of the pixel of added inputs ($I_p=I_A+I_B$). The functional relationships are given by eq.(11) and represented by the characteristic curves that are shown in Figs.5 and 6.

To obtain a specific logic function, the intensity ratio of the incident optical waves needs to be adjusted to an appropriate value. Fig.8b shows the input patterns I_A and I_B and the output fringe that corresponds to input state (I_A=0, I_B=0).

Fig.8c shows the realization of OR, XOR, NOR, and $\overline{\text{XOR}}$ logic gates by setting $\beta_A=\beta_B=1.0$. The phase shift $\Delta\phi_s$ of the coupled signal wave that corresponds to I_A or I_B is 0.971 π. Thus, the output fringe is shifted by an amount equal to $\Delta\phi_s$, and therefore, these gates are implemented at the positions of a quarter of a period simultaneously.

Table 1. Possible functions of two binary variables.

A	B	OR	XOR	NOR	$\overline{XOR}$	F	AND	T	NAND	B	$A\overline{B}$	$\overline{B}$	$\overline{A}+B$	A	$\overline{A}B$	$\overline{A}$	$A+\overline{B}$
0	0	0	0	1	1	0	0	1	1	0	0	1	1	0	0	1	1
0	1	1	1	0	0	0	0	1	1	1	0	0	1	0	1	1	0
1	0	1	1	0	0	0	0	1	1	0	1	1	0	1	0	0	1
1	1	1	0	0	1	0	1	1	0	1	0	0	1	1	0	0	1

To implement F, AND, T, and NAND logic gates, $\beta_A=\beta_B=3.5$ is selected. The phase shift $\Delta\phi_s$ of the coupled signal wave I_s that corresponds to I_A or I_B is $1.962\,\pi$. At appropriate regions F, AND, and their complements can be obtained as shown in Fig.8d.

To obtain the logic gates B, $A\overline{B}$, $\overline{B}$, and $\overline{A}+B$, $\beta_A=6.5$ and $\beta_B=41.0$ are selected. In this case, the phase changes of the output corresponding to I_A and I_B are $2.472\,\pi$ and $3.463\,\pi$, respectively. The logic operations are illustrated in Fig.8e.

When the intensities $\beta_A=41.0$ and $\beta_B=6.5$ are selected, the phase variations corresponding to I_A and I_B are $3.463\,\pi$ and $2.472\,\pi$, respectively. The logic gates A, $\overline{A}B$, $\overline{A}$, and $A+\overline{B}$ are obtained at the position of a quarter period simultaneously (Fig.8f).

Note that the system depicted in Fig.8a can realize up to four logic functions simultaneously. In the following, we present new system configurations based on employing two photorefractive crystals in cascade or parallel so that all logic gates can be implemented simultaneously.

(a) Two photorefractive crystals in cascade

The proposed system configuration is shown in Fig.9. Here, two output planes and two photorefractive crystals with different thicknesses d, applied electric field E_o, and angle θ are used. The output pump and signal intensities from the first crystal are calculated according to eq.(A23), and then the intensity ratio β_o at the input of the second crystal is calculated. If one chooses, $d_1=1.0$ cm, $\theta_1=1.25°$, and $Eo_1=18$ kV/cm, the logic gates F, AND, B, OR, T, NAND, $\overline{B}$, and NOR can be obtained at the first output plane (OP_1) if intensities $\beta_A=3.8$ and $\beta_B=6.5$ are selected (see Fig.10a). The phase variations corresponding to I_A and I_B are $2.288\,\pi$ and $2.545\,\pi$, respectively. Each gate is implemented at the positions of a 1/8 of a period simultaneously. For the second crystal, If we choose, $d_2=2.0$ cm, $\theta_2=1.75°$, and $Eo_2=19$ kV/cm, with intensities of $\beta_A=1.269$ and $\beta_B=2.170$. The phase shifts corresponding to I_A and I_B are 2.712π and $3.543\,\pi$, respectively. At appropriate regions on the second output plane (OP2) the logic gates $\overline{AB}$, XOR, $A\overline{B}$, A, $A+\overline{B}$, $\overline{XOR}$, $\overline{A}+B$, $\overline{A}$ can be obtained as shown in Fig 10b.

(b) Two photorefractive crystals in parallel

Fig.11 shows another system configuration using two photorefractive crystals in parallel to implement all the optical logic gates.

The parameters of the first crystal are $d_1=1.0$ cm, $\theta_1=2.8°$, and $Eo_1=13$ kV/cm; and for the second crystal, the parameter values are $d_2=2.1$ cm, $\theta_2=2.0°$, and $Eo_2=20$ kV/cm. When the intensities $\beta_A=3.3$ and $\beta_B=2.2$ are selected, the phase variations of the signal beam which passes through the first crystal corresponding to I_A and I_B are $1.482\,\pi$ and $1.268\,\pi$, respectively. When the signal passes through the second crystal, it gets phase shifts equal to $0.482\,\pi$ and $1.775\,\pi$ for the given values of β_A and β_B, respectively. The gates OR, XOR, $\overline{AB}$, F, NOR, $\overline{XOR}$, $A+\overline{B}$, T are obtained simultaneously in the first output (OP1) at appropriate regions (see Fig.12a). The other logic gates, (B, AND, A,

$A\bar{B}, \bar{B}$, NAND, $\bar{A}$ and $\bar{A}+B$) are obtained at the second output plane (OP2) (see Fig.12b).

CONCLUSIONS

We have presented a theoretical analysis based on the charge-transport model to predict the gain coefficient and signal phase shift for two-wave mixing in a photorefractive material subject to an external electric field. The results have been used as a guideline to implement real-time optical logic operations based on photorefractive two-wave mixing and fringe shifting technique that is executed by a Mach-Zehnder interferometer. New optical configurations have been proposed that employ two parallel or cascade photo-refractive crystals. These configurations can perform the sixteen basic two-operand logic functions simultaneously.

APPENDIX

The internal space-charge field induced by optical field for two-wave mixing in a photorefractive material subject to an applied external field E_o are derived using the set of equations used by Kukhtarev[14]:

Continuity eq.:

$$\frac{\partial}{\partial t}(N - N_D^+) = -\frac{\nabla \cdot J}{e} \qquad \text{(A1.a)}$$

Ion-rate eq.:

$$\frac{\partial N_D^+}{\partial t} = (\beta + sI)(N_D - N_D^+) - \gamma_R N N_D^+ \qquad \text{(A1.b)}$$

Current eq.

$$J = e N \mu E - k_B T \mu \nabla N + p I \qquad \text{(A1.c)}$$

Poisson's eq.:

$$\nabla \cdot \varepsilon E = e(N + N_A - N_D^+) \qquad \text{(A1.d)}$$

where N is the electron density, N_D is total density of photorefractive donors (both ionized and neutral). N_D may be an intentional or an unintentional dopant. N_D^+ is the density of ionized donors, which also act as traps. N_A is the density of negatively charged ions that compensate for the charge of N_D^+ in the dark and it is assumed to be constant and does not take part in the photorefractive process. $N_D - N_D^+$ is the density of neutral (filled) donors, J is the current density, β is the dark number-density generation rate, s is the photo cross section, I is total optical irradiance in the crystal, γ_R is the electron-trap recombination rate, μ is the mobility, p is the photovoltaic constant; ε is the static dielectric constant, E is the sum of the applied and the space-charge fields, n is the refractive index, n_o is the background refractive index of the crystal, E_{sc} is the magnitude of the space-charge field, and E_{opt} is the amplitude of the optical field.

Eliminate N_D^+ and N from eqs.(A1.a) and (A1.d) to obtain

$$\nabla \cdot \frac{\partial}{\partial t}(\varepsilon E) = -\nabla \cdot J \qquad \text{(A2)}$$

Since ε is independent of time, eq.(A2) may be integrated to yield

$$\frac{\partial E}{\partial t} = -\frac{J}{\varepsilon} + \frac{j}{\varepsilon} \qquad \text{(A3)}$$

where j/ε is the integration constant. jA is the current in the external circuit that is used to apply the external field E_o to the crystal over the area A of electrodes.

Next, both N_D^+ and J can be eliminated from eqs.(A1.a)-(A1.c) and (A3) to obtain

$$\frac{\partial E}{\partial t} = -\frac{1}{\varepsilon}(e\mu N E - k_B T \mu \nabla N + p I) + \frac{j}{\varepsilon} \qquad \text{(A4.a)}$$

$$\frac{\partial N}{\partial t} = (\beta + sI)N_D - (\beta + sI + \gamma_R N)(\frac{\varepsilon}{e}\nabla \cdot E - N - N_A) - \frac{1}{e}(e\mu E \cdot \nabla N + e\mu N \nabla \cdot E - k_B T \mu \nabla^2 N + \nabla \cdot pI) \qquad \text{(A4.b)}$$

Electrons trapped at the impurity sites absorb radiation at a rate proportional to the intensity distribution I and drift (or diffuse) through the crystal. Space-charge fields are generated that have the same periodicity as the optical interference

pattern. By the electro-optic effect, these fields induce the periodic index change that gives the crystal its diffraction properties. Hence, Equation (A4) is solved by assuming that N and **E** are of the form, ignoring higher-order harmonics,

$$N = N_o + N_2(z)e^{-jqy} + N_{-2}(z)e^{-jqy} \qquad (A5.a)$$

$$E = E_o + E_2(z)e^{jqy} + E_{-2}(z)e^{-jqy} \qquad (A5.b)$$

where $(E_{-2} = E_2^*)$, and q is the grating period given by,

$$q = |k_y - k_s| = 2k_y = 2n_o k_o \sin\theta \qquad (A6)$$

Since $q = 2\pi/\Lambda$, therefore, the fringe spacing (refractive-index grating period) is

$$\Lambda = \lambda_o / 2n_o \sin\theta \qquad (A7)$$

Substitution of eq.(A5) into eq.(A4) and retention of the lowest-order Bragg components yields

$$c\mu(N_o E_2 + N_2 E_o) \quad 2jk_y k_o T\mu N_2 - p_y a PS^* = 0 \qquad (A8.a)$$

$$saPS^* N_D + (\frac{c}{c} 2j k_y E_2 - N_2)(\beta + sI_o + \gamma_R N_o) +$$
$$(-N_A - N_o)(s a PS^* + \gamma_R N_2) -$$
$$\frac{2iky}{c}\left[e\mu(E_o N_2 + N_o E_2) - k_B T\mu \times 2i k_y N_2 + p_y a PS^*\right]$$
$$= 0 \qquad (A8.b)$$

$$(\beta + sI_o)N_D - (\beta + sI_o + \gamma_R N_o)(-N_A - N_o) = 0 \qquad (A8.c)$$

where I_o is the average optical intensity given by

$$I_o = a\left(|P|^2 + |S|^2\right) \qquad (A9.a)$$

and a is the square root of the ratio of the permittivity to the permeability, given by,

$$a = \frac{c\, n_o}{4\pi} \qquad (A9.b)$$

For irradiance typical of CW laboratory experiments[11]

$$N_o \approx \frac{(\beta + sI_o)(N_D - N_A)}{\gamma_R N_A} \qquad (A9.c)$$

Elimination of N_2 from eq.(A8.a) by using eq.(A8.b) yields

$$\frac{P S^*}{|P|^2 + |S|^2} +$$
$$\frac{E_2}{E_o - i E_d}\left[\frac{\beta + s I_o + \gamma_R N_o}{N_o}\frac{2 i k_y}{e}(E_o - i E_d) +\right.$$
$$\left.(\beta + s I_o + 2\gamma_R N_o) - \gamma_R N_A - \right]\frac{1}{\gamma_R N_A} = 0 \qquad (A10)$$

Again, for typical irradiance, $\frac{\beta + s I_o + \gamma_R N_o}{\beta + s I_o + 2\gamma_R N_o} << 1$, neglecting dark generation of carriers (β) compared with photogeneration (sI_o), and assuming that $N_A/N_D << 1$ one obtains

$$E_2 = \frac{-(E_o - i E_d)}{A}\frac{P S^*}{|P|^2 + |S|^2} \qquad (A11)$$

where $A = 1 + \frac{E_d}{E_q} + i\frac{E_o}{E_q}$

Recall that the scalar wave equation is given by,

$$\frac{\partial^2 E_{opt}}{\partial z^2} + (\frac{2\pi}{\lambda_o})^2 n^2 E_{opt} = 0 \qquad (A12)$$

where λ_o is the wavelength in the vacuum, and n is given by

$$n = n_o + \Delta n \qquad (A13)$$

Using Δn defined by eq.(1), where E is total electric field ($E = E_o + E_{sc}$) and omit the term $n_o^2 r_{41} E$ relative to n_o^2 to obtain

$$n^2 = n_o^2 (1 + n_o^2 r_{41} E) \qquad (A14)$$

Substitution of eqs.(A5), (8) and (A14) into the wave equation yields,

$$(-k_z^2 P - 2jk_z P' + P'')e^{-ik_p \cdot r} +$$
$$(-k_z^2 S - 2jk_z S' + S'')e^{-ik_s \cdot r} +$$
$$(\frac{2\pi}{\lambda_o})^2 n_o^2 \left[1 + n_o^2 r_{41}(E_o + E_2 e^{jqy} + E_{-2} e^{-jqy})\right]$$
$$\left[P e^{-ik_p \cdot r} + S e^{-ik_s \cdot r}\right] = 0 \qquad \text{(A15)}$$

As usual, the waves generated in the directions $\mathbf{k}_p + \mathbf{k}_s$ and $\mathbf{k}_p - \mathbf{k}_s$ are neglected, and the changes in P(z,t) and S(z,t) with respect to z are assumed to be very slow, so the second derivatives of P(z,t) and S(z,t) with respect to z are neglected. Then, the following coupled differential equations

$$P' - i\delta(P E_o + E_2 S) = 0 \qquad \text{(A16.a)}$$
$$S' - i\delta(S E_o + E_{-2} P) = 0 \qquad \text{(A16.b)}$$

where δ is the electro-optic activity define by eq.(2). These equations may be conveniently recast in terms of their real and imaginary parts, with the result,

$$I_p' + 2\delta\, \mathrm{Im}\left[\frac{-(E_o - iE_d)}{A}\right]\frac{I_p I_s}{I_o} = 0 \qquad \text{(A17.a)}$$
$$\varphi_p' - \delta\left[E_o + \mathrm{Re}\left(\frac{-(Eo - iEd)}{A}\right)\right]\frac{I_s}{I_o} = 0 \qquad \text{(A17.b)}$$
$$I_s' - 2\delta\, \mathrm{Im}\left[\frac{-(E_o - jE_d)}{A}\right]\frac{I_p I_s}{I_o} = 0 \qquad \text{(A17.c)}$$
$$\varphi_s' - \delta\left[E_o + \mathrm{Re}\left(\frac{-(Eo - iEd)}{A}\right)\right]\frac{I_p}{I_o} = 0 \qquad \text{(A17.d)}$$

Let the intensity gain factor Γ be defined as,

$$\Gamma = 2\delta\, \mathrm{Im}\left[\frac{-(E_o - iE_d)}{A}\right] \qquad \text{(A18.a)}$$

Therefore,

$$\Gamma = 2\delta E_d \frac{1 + E_d/E_q + E_o^2/E_d E_q}{(1 + E_d/E_q)^2 + (E_o/E_q)^2} \qquad \text{(A18.b)}$$

Let the phase conversion factor γ be defined as

$$\gamma = \delta\, \mathrm{Re}\left[\frac{-(E_o - iE_d)}{A}\right] \qquad \text{(A18.c)}$$

Hence,

$$\frac{\gamma}{\Gamma} = \frac{\mathrm{Cot}\,\phi_g}{2} \qquad \text{(A18.d)}$$

where

$$\phi_g = \tan^{-1}\left[\frac{E_d(1 + E_d/E_q + E_o^2/E_d E_q)}{E_o}\right] \qquad \text{(A18.e)}$$

Using these factors, we can rewrite eq.(A17) into the form

$$I_p' + \Gamma\frac{I_p I_s}{I_o} = 0 \qquad \text{(A19.a)}$$
$$I_s' - \Gamma\frac{I_p I_s}{I_o} = 0 \qquad \text{(A19.b)}$$
$$\varphi_p' - \gamma\frac{I_s}{I_o} - \delta E_o = 0 \qquad \text{(A19.c)}$$
$$\varphi_s' - \gamma\frac{I_p}{I_o} - \delta E_o = 0 \qquad \text{(A19.d)}$$

Subtract eq.(A19.b) from eq.(A19.a) we get,

$$I_p' - I_s' + \frac{2\Gamma}{I_o} I_p I_s = 0 \qquad \text{(A20)}$$

Let $\Delta = I_p - I_s$ and $\Delta' = I_p' - I_s'$, then integrating both sides of eq.(A20) to get

$$\Delta = I_o \tanh Q(z,t) \qquad \text{(A21)}$$

where

$$Q(z,t) = -\frac{\Gamma z}{2} + \tanh^{-1}\frac{\Delta_o}{I_o}$$

This leads to

$$I_p = \frac{I_o}{2}\left[1 + \tanh Q(z,t)\right] \qquad \text{(A22.a)}$$
$$I_s = \frac{I_o}{2}\left[1 - \tanh Q(z,t)\right] \qquad \text{(A22.b)}$$

Then some straightforward algebra gives

$$I_p = \frac{I_o \beta_o}{\beta_o + e^{\Gamma d}} \qquad \text{(A23.a)}$$
$$I_s = \frac{I_o e^{\Gamma d}}{\beta_o + e^{\Gamma d}} \qquad \text{(A23.b)}$$

where d is the thickness of the crystal; β_o is the beam intensity ratio at z=0

$$\beta_0 \simeq \left.\frac{I_p}{I_s}\right|_{z=0} \qquad \text{(A24)}$$

The phase shift of the signal beam $\Delta\varphi_s = \varphi_s(d) - \varphi_s(0)$ can be obtained by integrating both sides of eq.(A19.d) to yields

$$\Delta\varphi_s = \delta E_0\, d + \frac{\gamma}{\Gamma}\ln\left[\frac{(\beta+1)e^{\Gamma d}}{\beta+e^{\Gamma d}}\right] \qquad \text{(A25)}$$

REFERENCES

1. A.V. Krishnamooorthy, A.L. Lenttine, K.W. Goossev, J.A. Walker, T.K. Woodward, "3-D integration of MQW modulators over active submicron CMOS circuits: 375 Mb/s transimpedance receiver-transmitter circuit." IEEE Photon. Technol. Lett. Vol.7, pp.1288-1290, 1995.
2. Y. Yuan, X. Zhang, P. Bhattacharyu, "Low photocurrent GaAs-$Al_{0.3}Ga_{0.7}As$ Multiple-Quantum-Well modulators with selective Erbium doping." IEEE Photon. Technol. Lett. Vol.8, pp.1638-1643, 1996.
3. H. Kosaka, M. Kajita, Y. Li, and Y. Sugimoto, 'A two-dimensional optical parallel transmission using a vertical-cavity surface-emitting laser array module and an image fiber." IEEE Photon. Technol. Lett. Vol.9, pp.253-255, 1997
4. A.A. Kamshilin, J. Frejlich, and P.M. Garcia, "Electrophotochromic gratings in photorefractive $Bi_{12}TiO_{20}$ crystals." Appl. Opt. Vol.31, pp.1787-1793, 1992.
5. F. Vachss, J. Hong, S. Campbell, and D. Cordeiro, "Stable photorefractive square-low conversion using moving grating techniques." Appl. Opt. Vol.31, pp.1783-1786, 1992.
6. T. Tschudi, A. Herden, J. Goltz, H. Klumb, F. Laeri, and J. Albers, "Image amplification by two- and four-wave mixing in $BaTiO_3$ photorefractive crystals." IEEE J. Quantum Electron. Vol.22, pp.1493-1502, 1986.
7. J. Joseph, K. Kamra, K. Singh, and P.K.C. Pillai, "Real-time image processing using relative erasure in photorefractive two-wave mixing." Appl. Opt. Vol.31, pp.4769-4772, 1992.
8. T.Y. Chang, J.H. Hong, and P. Yeh, "Spatial amplifications image-processing techniques using the selective amplification of spatial frequencies." Opt. Lett. Vol.15, pp.743-745, 1990.
9. G.C. Vally and M.B. Klein, "Optical properties of photorefractive materials for optical data processing." Opt. Eng. Vol.22, pp.704-711, 1983.
10. N.A. Vainos, S.L. Clapham, and R.W. Eason, "Multiplexed permanent and real-time holographic recording in photorefractive BSO." Appl. Opt. Vol.28, pp.4381-4355, 1989.
11. G.C. Vally, "Two-wave mixing with an applied field and a moving grating." J. Opt. Soc. Am. Vol.1, pp.868-873, 1984.
12. M.Z. Zha, P. Amrhein, and P. Gunter, "Measurement of phase shift of photorefractive gratings by a novel method." IEEE J. Quantum Electron. Vol.26, pp.788-792, 1990.
13. H. Xu, Y. Yuan, K. Xu, and Y. Lu, "Real-time parellel optical logic operation using photorefractive two-wave mixing and fringe-shifting techniques." Appl. Opt. Vol.31, pp.1769-1773, 1992.
14. N.V. Kukhtarev, V.B. Markov, S.G. Odulov, M.S. Soskin, and V.L. Vinetskii, "Holographic storage in electro-optic crystals. I: Steady state." Ferroelectrics, Vol.22, pp.949-960, 1979.

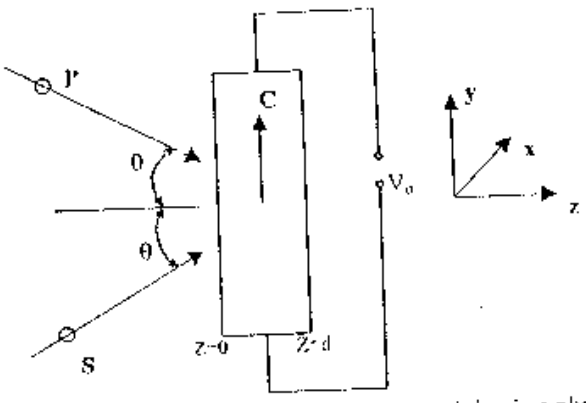

Fig.1. A schematic representation of the two-wave mixing in a photorefractive crystal.

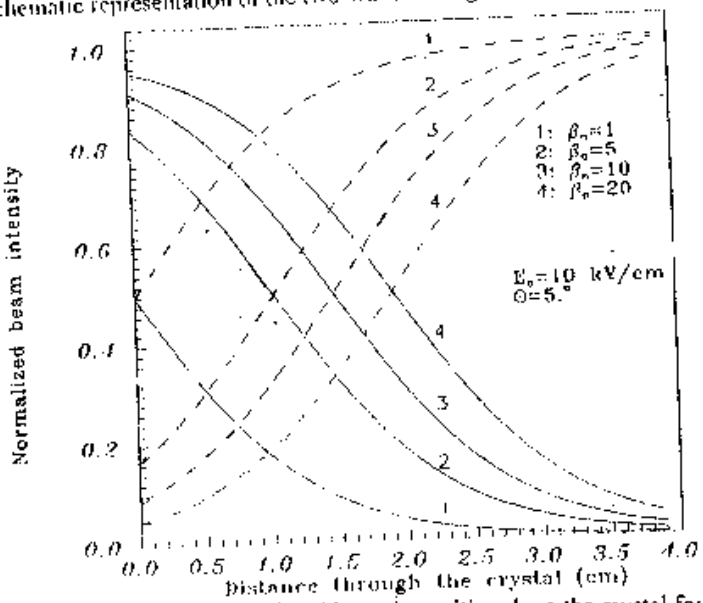

Fig.2 The distribution of pump and signal beam intensities along the crystal for different intensity beam ratios. ——— I_p/I_{0p}, - - - - I_s/I_{0s}

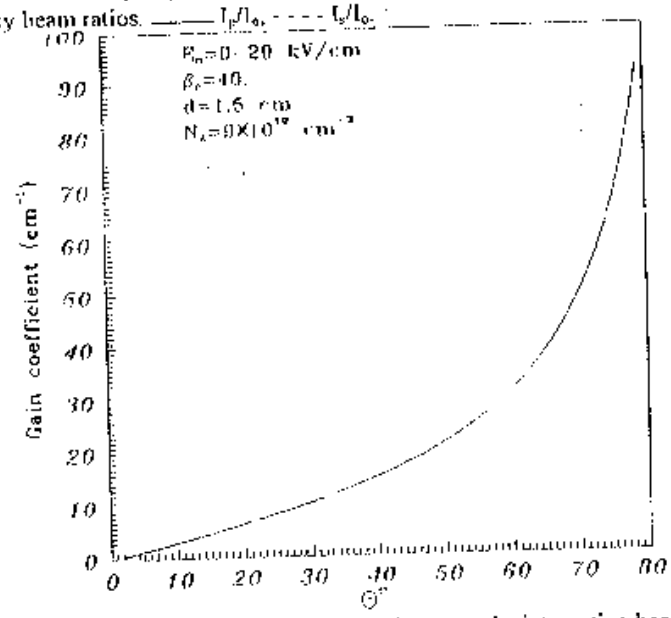

Fig.3 Gain coefficient Γ as a function of the angle between the interacting beams θ.

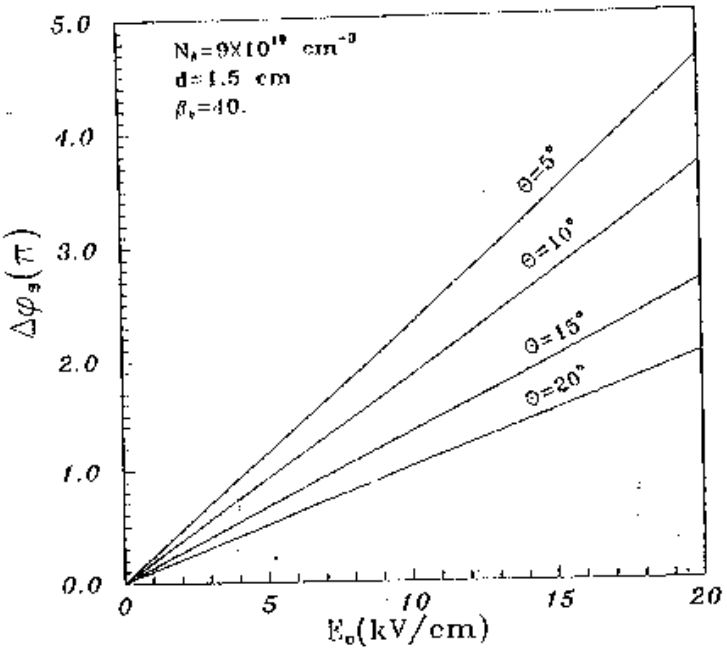

Fig.6. Electric field dependence of the signal phase shift for different values of θ

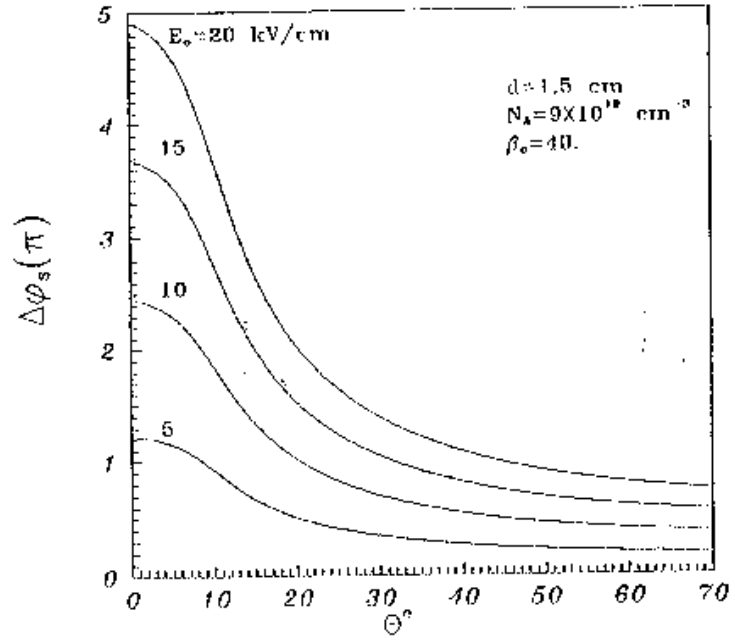

Fig.7. Signal phase shift as a function of the angle between the incident interacting beams.

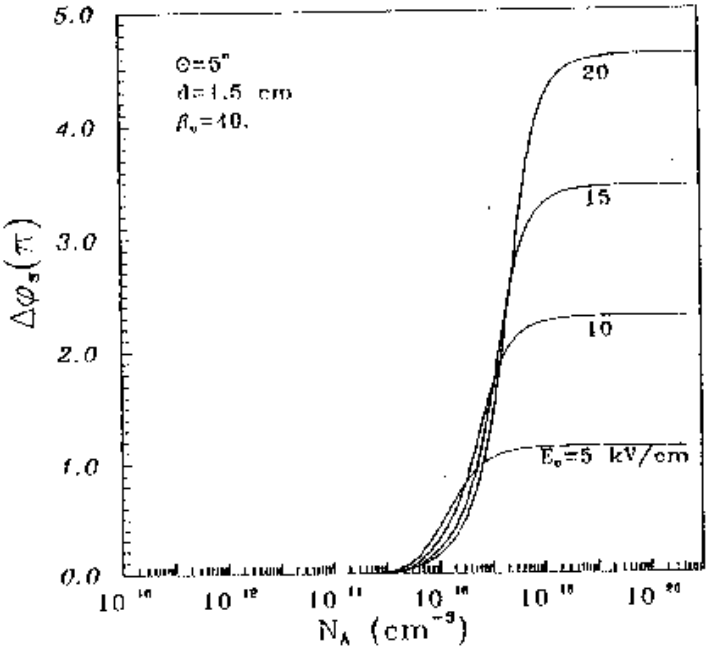

Fig 4. Dependence of signal phase shift on trap density for different applied fields.

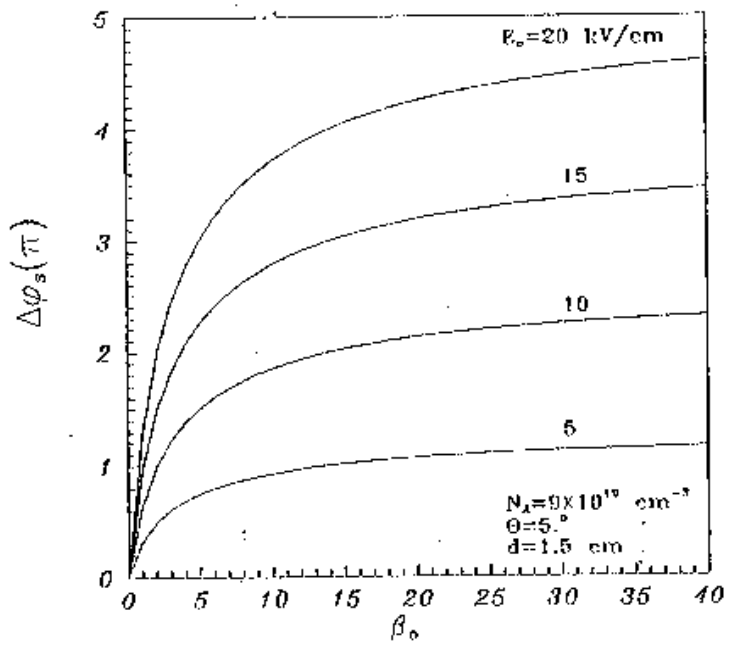

Fig 5. Signal phase shift versus intensity beam ratio and taking the applied field as independent parameter..

(a)

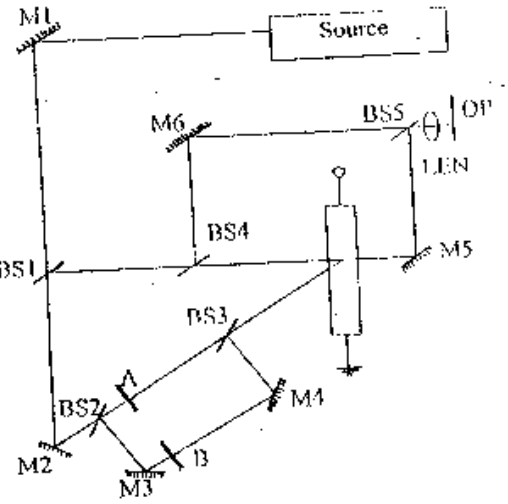

(b)

(c)

A	B	S_1	S_2	S_3	S_4
0	0	0	0	1	1
0	1	1	1	0	0
1	0	1	1	0	0
1	1	1	0	0	1
		OR	XOR	NOR	$\overline{XOR}$

(d)

A	B	S_1	S_2	S_3	S_4
0	0	0	0	1	1
0	1	0	0	1	1
1	0	0	0	1	1
1	1	0	1	1	0
		F	AND	T	NAND

(e)

A	B	S_1	S_2	S_3	S_4
0	0	0	0	1	1
0	1	1	0	1	1
1	0	0	1	1	0
1	1	1	0	0	1
		B	$A\overline{B}$	$\overline{B}$	$\overline{A}+B$

(f)

A	B	S_1	S_2	S_3	S_4
0	0	0	0	1	1
0	1	0	1	1	0
1	0	1	0	0	1
1	1	1	0	0	1
		A	$\overline{A}B$	$\overline{A}$	$A+\overline{B}$

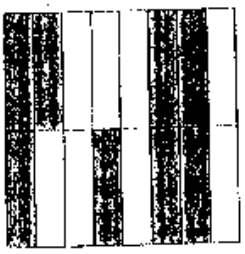

Fig.8. (a) A system configuration for implementing optical logic operations
(b) Input patters and output interference fringe corresponding to input state (0,0).
(c) Realization of logic gates OR, XOR, NOR, and $\overline{XOR}$.
(d) Realization of logic gates F, AND, T, and NAND.
(e) Realization of logic gates B, $A\overline{B}$, $\overline{B}$, and $\overline{A}+B$.
(f) Realization of logic gates A, $\overline{A}B$, $\overline{B}$, and $\overline{A}+B$.

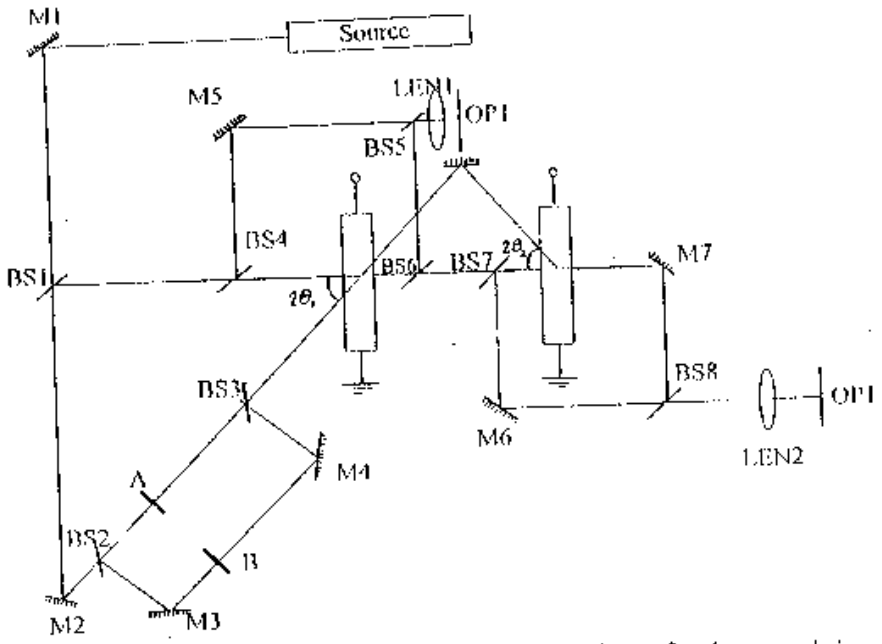

Fig.9. A proposed system configuration that uses two photorefractive crystals in cascade

A	B	S_1	S_2	S_3	S_4	S_5	S_6	S_7	S_8
0	0	0	0	0	0	0	1	1	1
0	1	0	0	1	1	1	1	0	0
1	0	0	0	0	1	1	1	0	0
1	1	0	1	1	1	1	0	0	0
		F	AND	B	OR	T	NAND	$\overline{B}$	NOR

(a)

A	B	S_1	S_2	S_3	S_4	S_5	S_6	S_7	S_8
0	0	0	0	0	0	1	1	1	1
0	1	1	1	0	0	1	0	1	1
1	0	0	1	1	1	1	0	0	0
1	1	0	0	0	1	1	1	1	0
		$\overline{A}B$	XOR	$A\overline{B}$	A	$A+\overline{B}$	$\overline{XOR}$	$\overline{A}+B$	$\overline{A}$

(b)

Fig.10. Realization of logic gates using two crystals in cascade.
(a) F, AND, B, OR, T, NAND, $\overline{B}$, and NOR gates at OP1.
(b) $\overline{A}B$, XOR, $A\overline{B}$, A, $A+\overline{B}$, $\overline{XOR}$, $\overline{A}+B$, and $\overline{A}$ gates at OP2

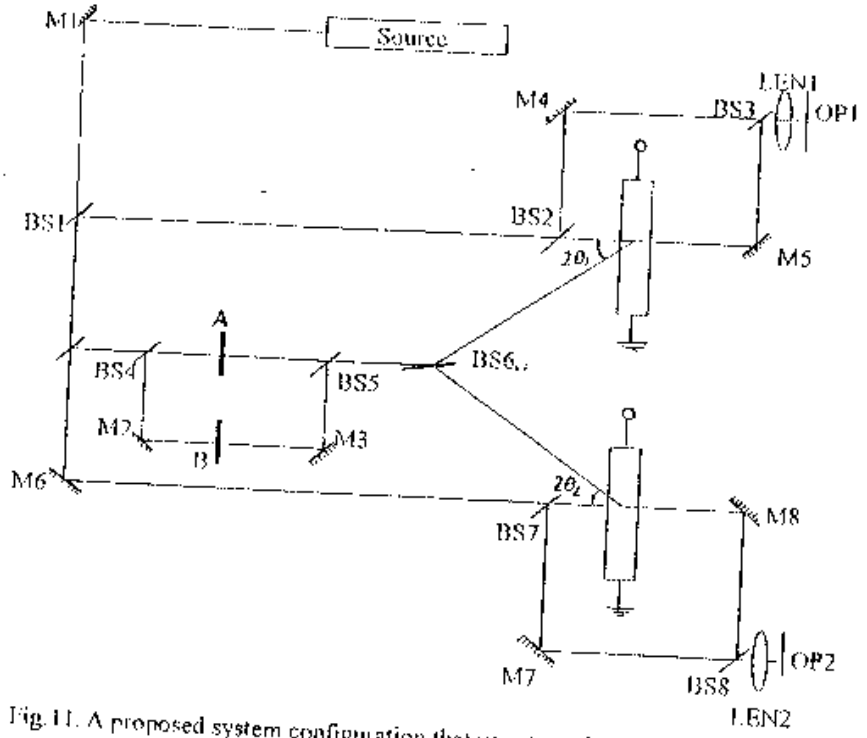

Fig. 11. A proposed system configuration that uses two photorefractive crystals in parallel.

$\overline{A}$	$\overline{B}$	$\overline{S_1}$	$\overline{S_2}$	$\overline{S_3}$	$\overline{S_4}$	$\overline{S_5}$	$\overline{S_6}$	$\overline{S_7}$	$\overline{S_8}$
0	0	0	0	0	0	1	1	1	1
0	1	1	1	1	0	0	0	0	1
1	0	1	1	0	0	0	0	1	1
1	1	1	0	0	0	0	1	1	1
		OR	XOR	$\overline{A}B$	F	NOR	$\overline{XOR}$	$A+\overline{B}$	T

(a)

$\overline{A}$	$\overline{B}$	$\overline{S_1}$	$\overline{S_2}$	$\overline{S_3}$	$\overline{S_4}$	$\overline{S_5}$	$\overline{S_6}$	$\overline{S_7}$	$\overline{S_8}$
0	0	0	0	0	0	1	1	1	1
0	1	1	0	0	0	0	1	1	1
1	0	1	0	1	1	1	1	0	1
1	1	1	1	1	0	0	0	0	1
		B	AND	A	$A\overline{B}$	$\overline{B}$	NAND	$\overline{A}$	$\overline{A}+B$

(b)

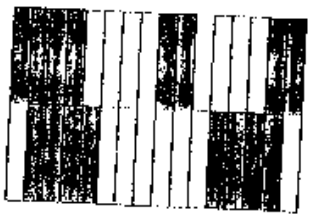

Fig. 12. Realization of logic gates using two crystals in parallel.
(a) OR, XOR, $\overline{A}B$, F, NOR, $\overline{XOR}$, $A+\overline{B}$, and T gates at OP1.
(b) B, AND, A, $A\overline{B}$, $\overline{B}$, NAND, $\overline{A}$, and $\overline{A}+B$ gates at OP2.